Input-specific localization of NMDA receptor GluN2 subunits in thalamocortical neurons

Mackenzie A. Topolski[1], Brian L. Gilmore[1], Rabeya Khondaker[1,2], Juliana A. Michniak[1,3], Carleigh Studtmann[1,2], Yang Chen[1,2], Gwen N. Wagner[1], Aaron E. Pozo-Aranda[1,4], Shannon Farris[1,5,6], Sharon A. Swanger[1,5,6*]

[1]Fralin Biomedical Research Institute at VTC, Virginia Tech, Roanoke, VA, USA
[2]Graduate Program in Translational Biology, Medicine, and Health, Virginia Tech, Blacksburg, VA, USA.
[3]Department of Biological Systems Engineering, Virginia Tech, Blacksburg, VA, USA
[4]School of Neuroscience, Virginia Tech, Blacksburg, VA, USA
[5]Department of Biomedical Sciences and Pathobiology, Virginia-Maryland College of Veterinary Medicine, Virginia Tech, Blacksburg, VA, USA.
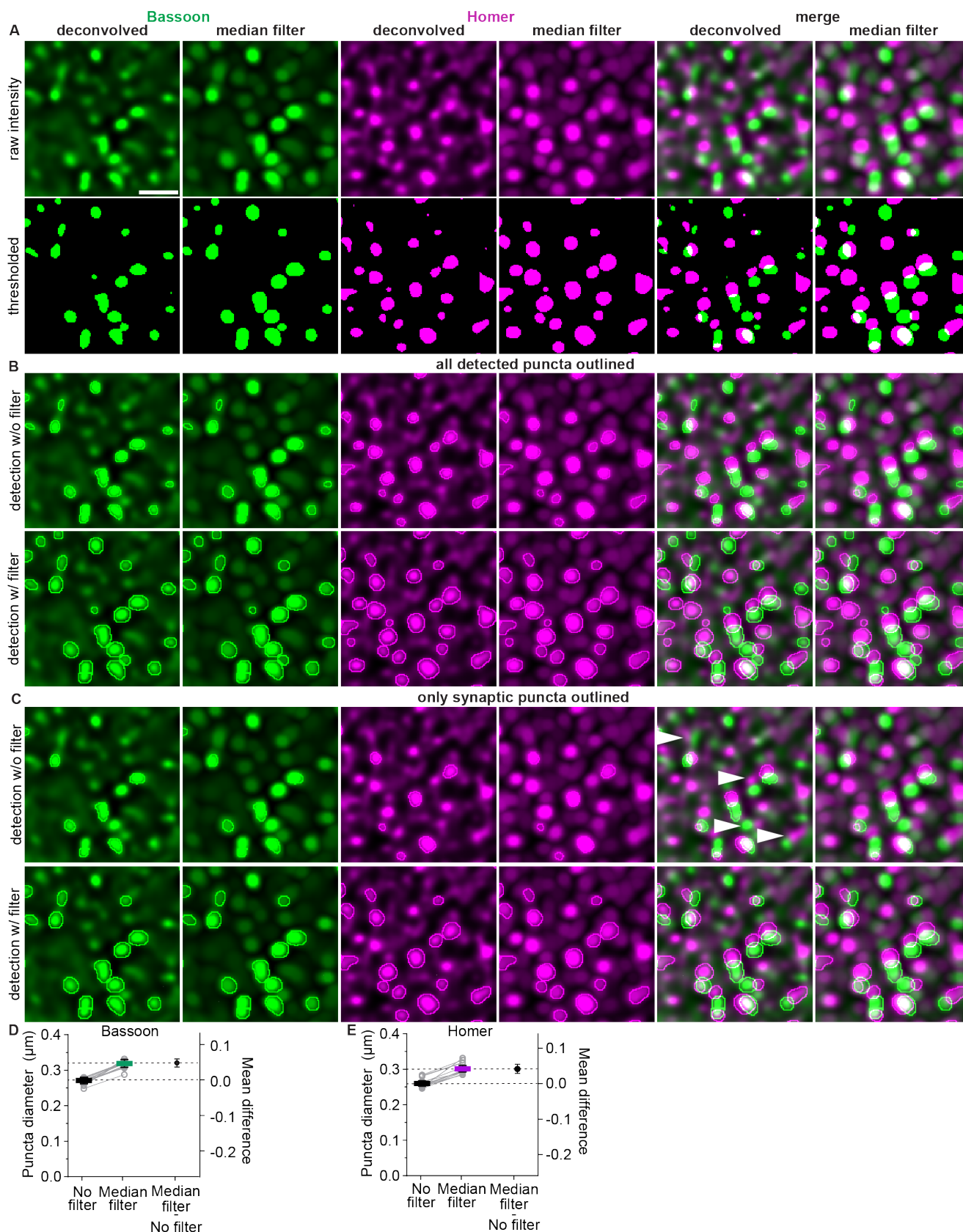[6]Department of Internal Medicine, Virginia Tech Carilion School of Medicine, Roanoke, VA, USA.

*Corresponding Author: Sharon A. Swanger (saswanger@vtc.vt.edu)

Supplementary Material:

Supplementary Figures S1 – S11

Supplementary Table S1

Supplemental Figure S1. Synapse detection with median filter. A. 60x (4x SoRa) images show the effect of a median filter with a 2-pixel radius on bassoon and homer signal. The original deconvolved image is shown next to the same image with a median filter applied. The top row shows the raw intensity and the bottom row is thresholded at the levels utilized for synapse detection. **B.** Raw intensity images from panel A are shown with (B) all detected puncta outlined and (C) only homer/bassoon synaptic puncta

outlined without and with the median filter. Estimation plots show (D) bassoon and € homer puncta without and with the median filter on the left y-axis (mean ± SD) and the mean difference on the right y-axis with 95% CI.
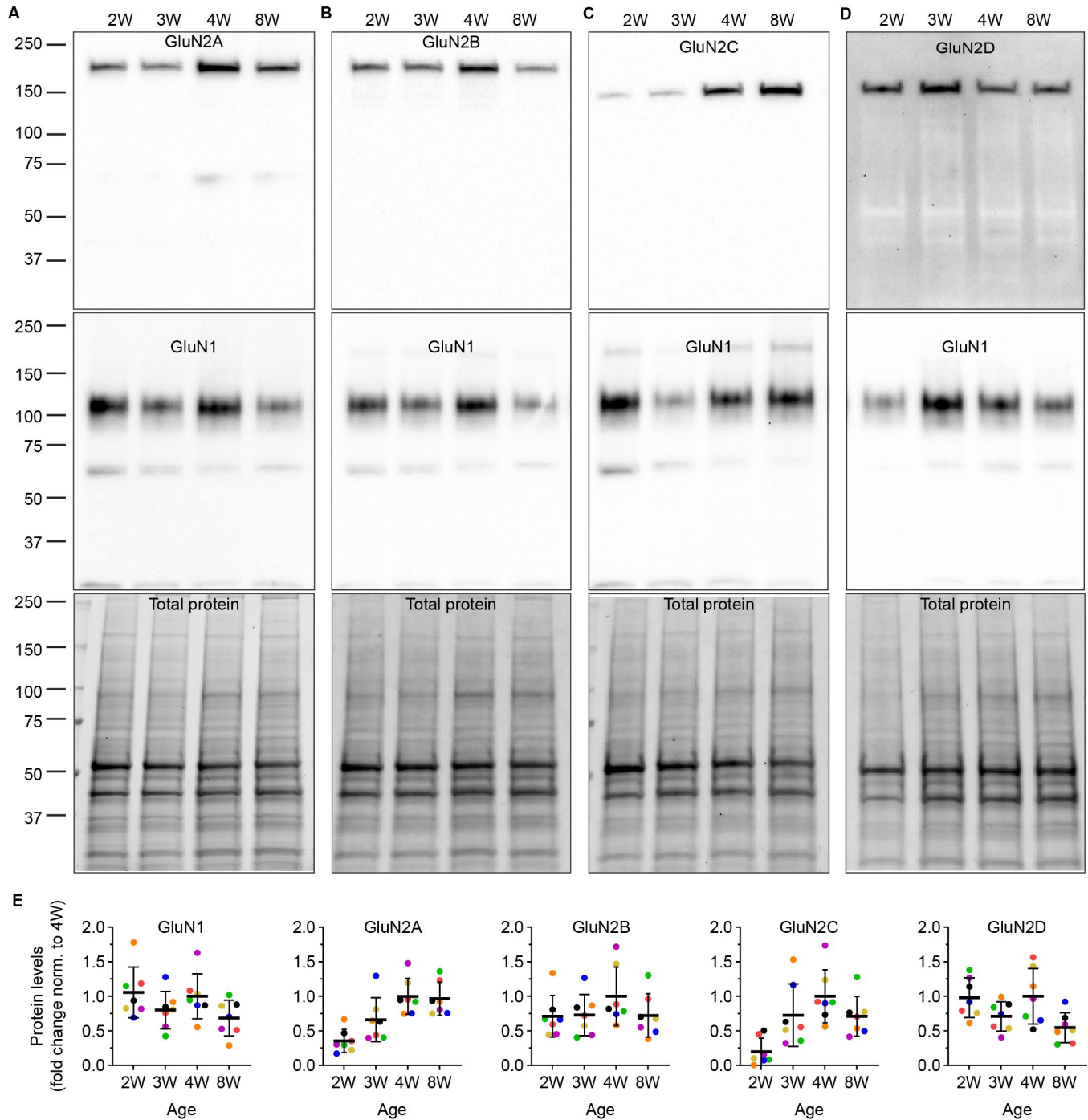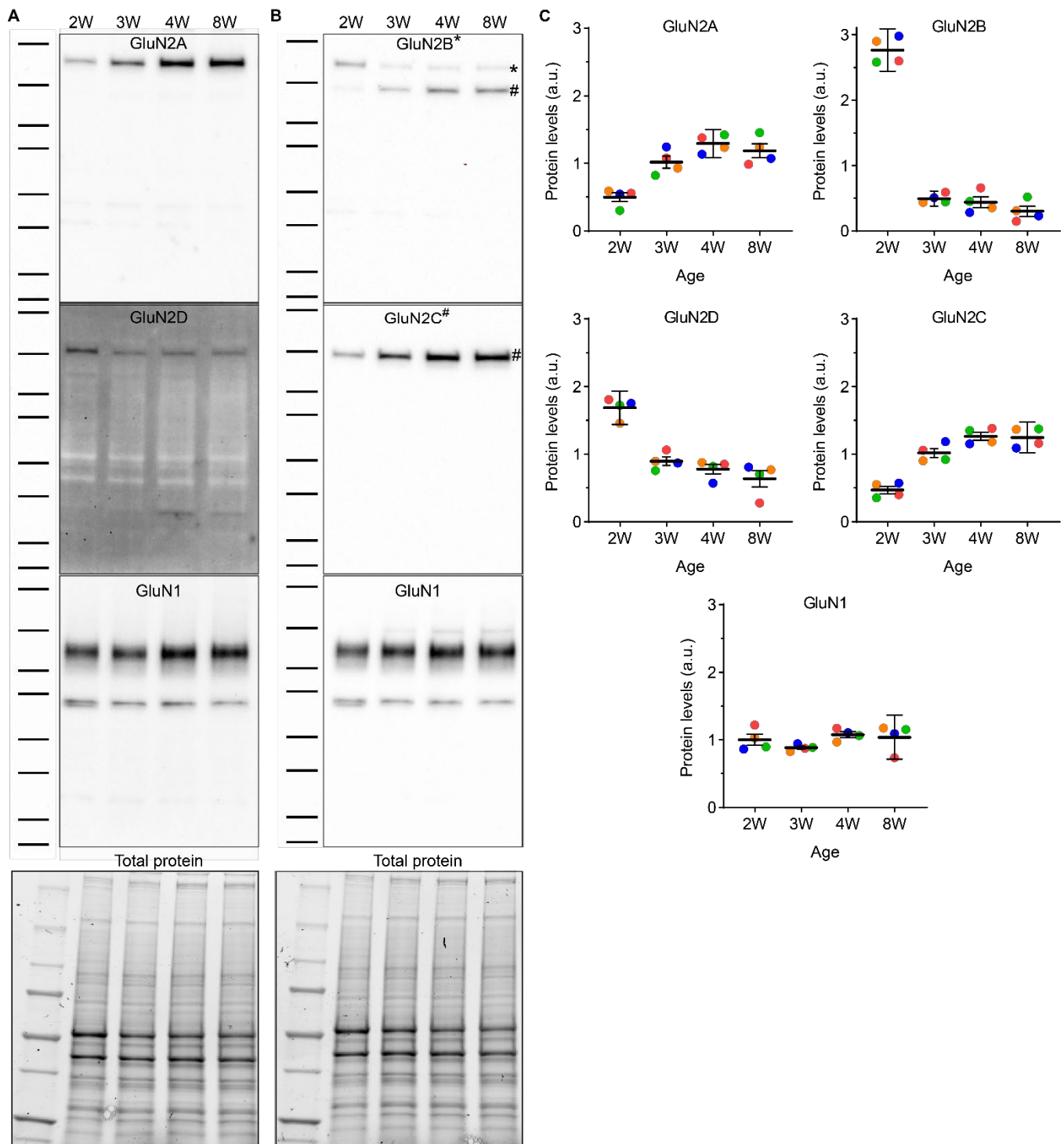

Supplemental Figure S2. Developmental expression of GluN subunits in the thalamus. VB thalamus tissue punches from C57Bl/6J mice aged 2, 3, 4, and 8 weeks (W) were homogenized, processed for SDS PAGE, run on duplicate gels, and then samples were immunoblotted for NMDAR subunits ($n = 7$ mice; 2W: sex unknown; 3W: 3F, 4M; 4W: 5M, 2F; 8W: 3M, 4F). Samples were probed for (**A**) GluN2A, (**B**) GluN2B, (**C**) GluN2C, and (**D**) GluN2D as well as GluN1 (middle, **A** – **D**). **E.** Protein levels were quantified by densitometry and normalized to total protein (bottom, **A** – **D**) within each gel. Protein levels for each replicate were shown as individual data points of the same color across age and expressed as fold change from the 4W mean to control for differences in band intensity across experiments. The line and error bars are mean ± SD.
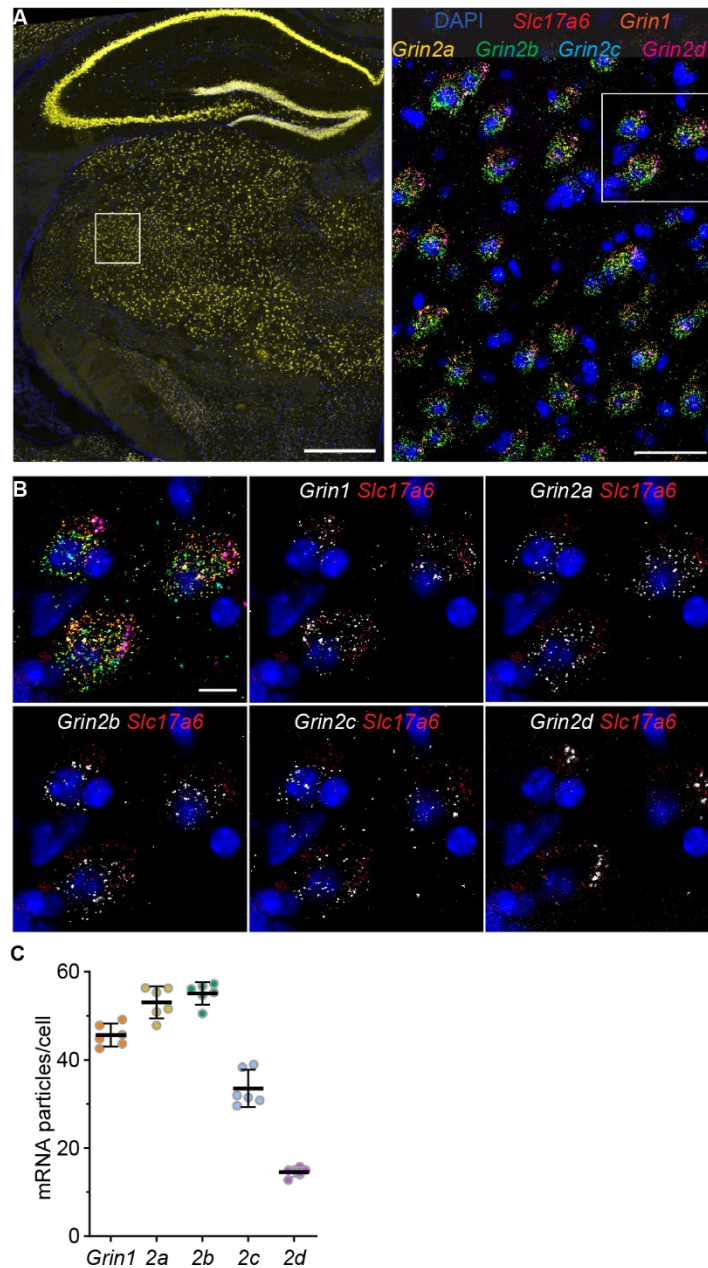
Supplemental Figure S3. GluN subunit mRNA expression levels differ in the VPM thalamus. A. Tiled 40x image of a fixed mouse brain section shows RNAscope detection of *Grin2a* mRNA (yellow) and DAPI-stained nuclei (blue). **B.** The boxed region from panel A shows a 40x image of *Grin1, Grin2a, Grin2b, Grin2c, Grin2d,* and *Slc17a6* (red) mRNA with DAPI. **C.** Images of the boxed region from panel B depict the merged signals as well as each *Grin* gene along with *Slc17a6* mRNA and DAPI. **D.** The plot shows the mean mRNA particle number per neuron (averaged across approx. 30 neurons per mouse) for 6 mice with the group mean ± *SD*. Scale bars: (A) 500 μm, (B) 40 μm, and (C) 10 μm.
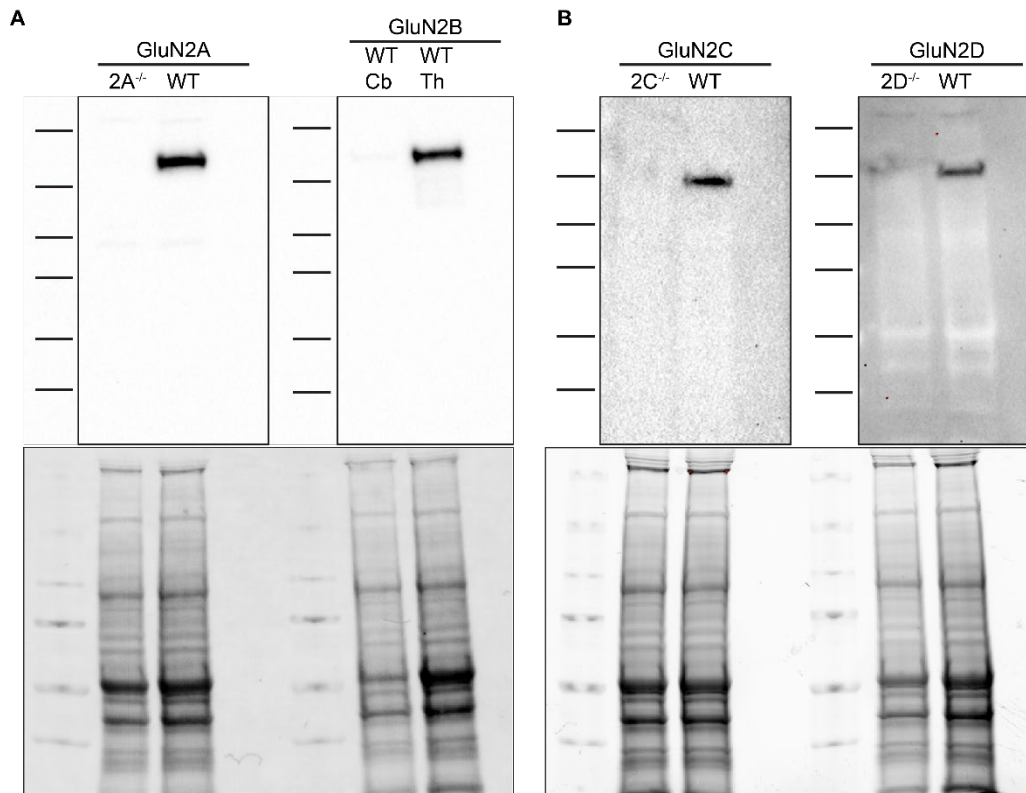
Supplemental Figure S4. Validation of GluN2 antibodies for western blotting. A. At left, whole thalamus from WT and *Grin2a* null (2A$^{-/-}$) mice were homogenized and separated by SDS PAGE, and then immunoblotted with GluN2A antibodies. At right, whole thalamus (Th) from 4-week-old WT mice and whole cerebellum (Cb) from 12-week-old mice were homogenized and separated by SDS PAGE, and then immunoblotted with GluN2B antibodies. **B**. Thalamus from WT mice as well as *Grin2c* null (2C$^{-/-}$) mice (left) and *Grin2d* null (2D$^{-/-}$) mice were processed as in panel A, and then immunoblotted with GluN2C and GluN2D antibodies, respectively. Total protein signals from each gel are shown at the bottom of panels A and B.

Supplemental Figure S5. Developmental expression of NMDAR subunits in the cerebellum. Whole cerebellum from mice aged 2, 3, 4, and 8 weeks (W) were homogenized, processed for SDS PAGE, run on duplicate gels, and then samples were immunoblotted. Samples were probed for (**A**) GluN2A, GluN2D, and GluN1, and (**B**) GluN2B, GluN2C, and GluN1. In the top image of panel B, the higher band (*) is GluN2B and the lower band is residual GluN2C (#) not removed by stripping buffer prior to probing for GluN2B. Protein levels were quantified by densitometry and normalized to GluN1 levels as well as total protein within each gel. **C**. Protein levels for each replicate ($n = 4$ mice; 2F, 2M) were shown as individual data points of the same color across age and expressed as fold change from the mean intensity across all ages to control for differences in band intensity across experiments. The line and error bars are mean ± SD.
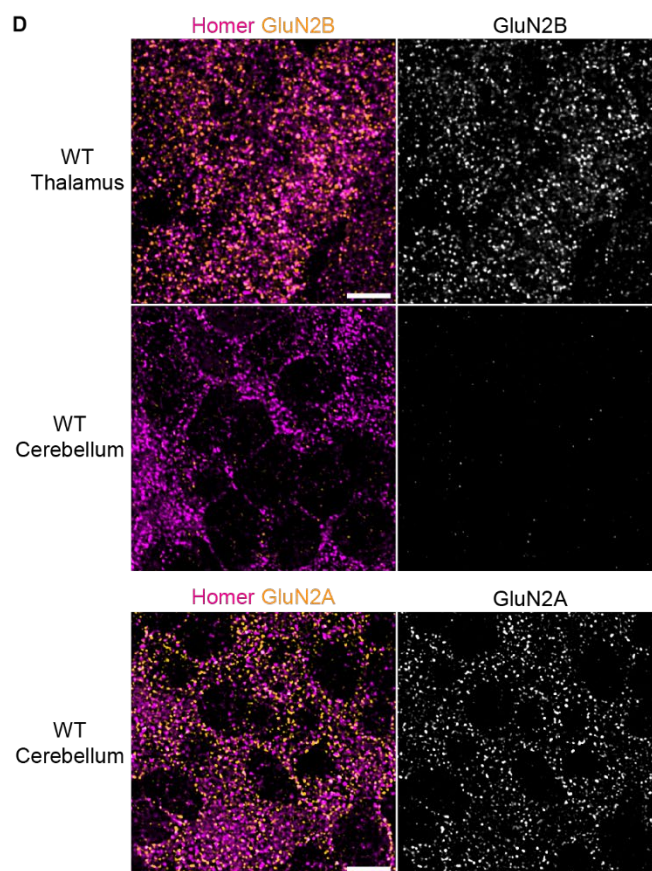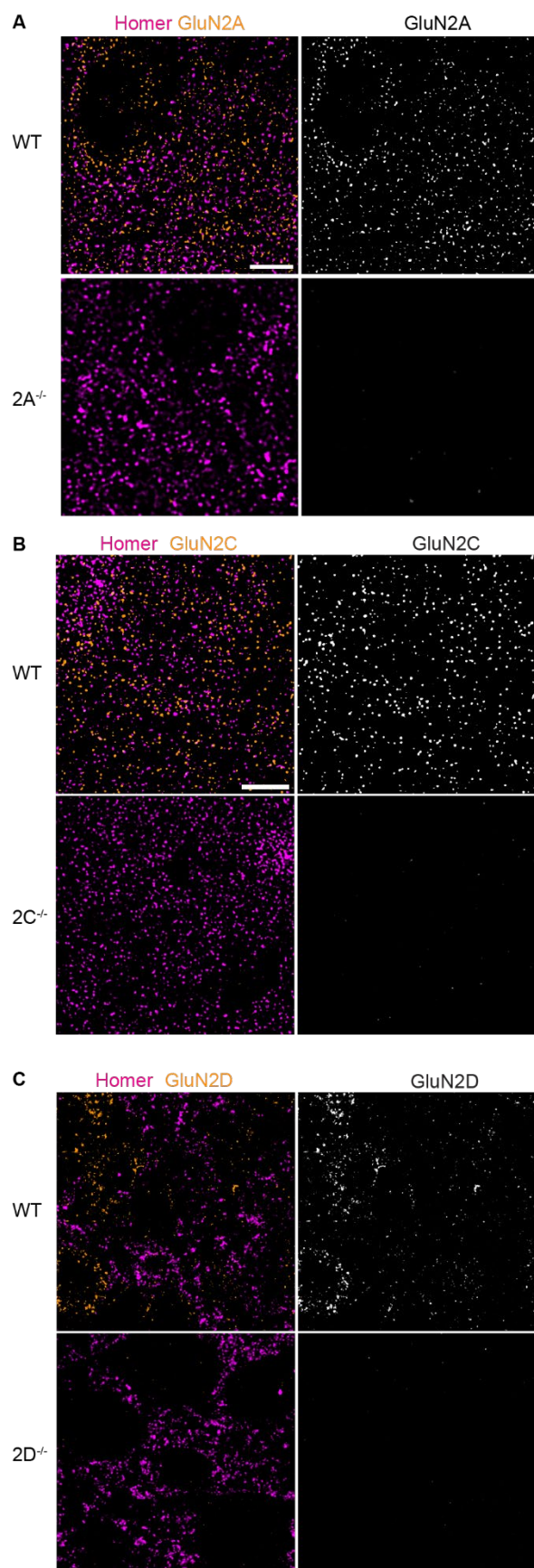
Supplemental Figure S6. Validation of GluN2 antibodies for immunohistochemistry. 60x (4x SoRa) images of VPM thalamus are shown for: (**A**) WT and *Grin2a* null (2A$^{-/-}$) mice immunostained for homer and GluN2A, (**B**) WT and *Grin2c* null (2C$^{-/-}$) mice immunostained for homer and GluN2C, and (**C**) WT and *Grin2d* null (2D$^{-/-}$) mice immunostained for homer and GluN2D. (**D**) 60x (4x SoRa) images show VPM thalamus and the cerebellar granule cell layer from 12-week-old WT mice immunostained for homer and GluN2B as well as the cerebellar granule cell layer immunostained for homer and GluN2A to show the distribution of a highly expressed GluN2 subunit in this region. Scale bars: 5 μm.
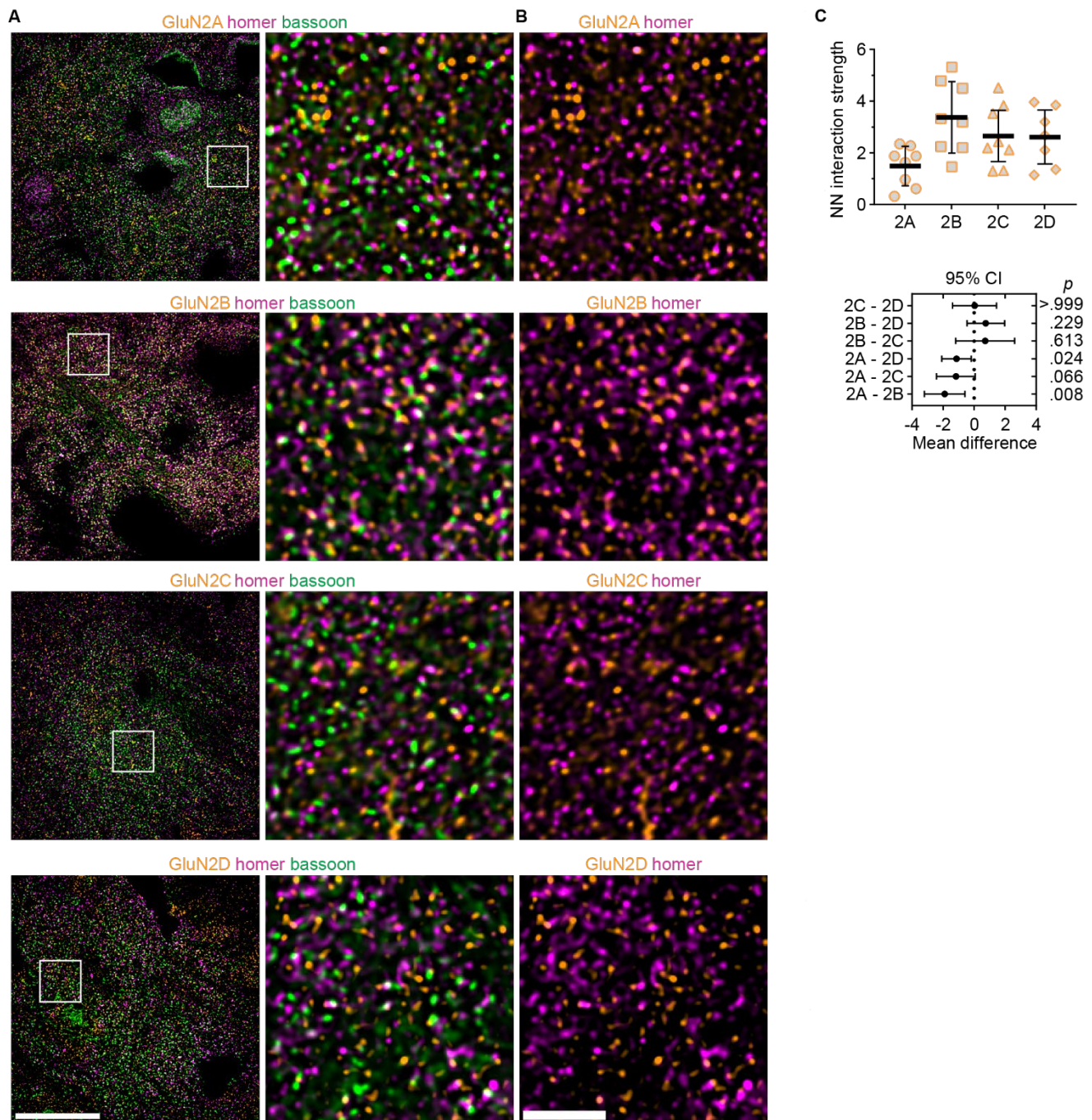
Supplemental Figure S7. GluN2-homer nearest neighbor analysis. A. 60x (4x SoRa) images show GluN2, homer, and bassoon immunolabeling with the boxed region shown at right. **B**. GluN2 and homer signals are shown to highlight their relative spatial distributions. **C.** NN interactions strengths were plotted for each mouse with group mean ± *SD*. Groups were compared by a mixed-effects model and Tukey's pairwise comparison tests for which the 95% CI of the mean difference and *p* values are shown beneath the group data. F (1.89, 12.6) = 7.08, p = 0.009, n = 8 mice (4F, 4M). Scale bars: A) 20 µm; B) 3 µm.
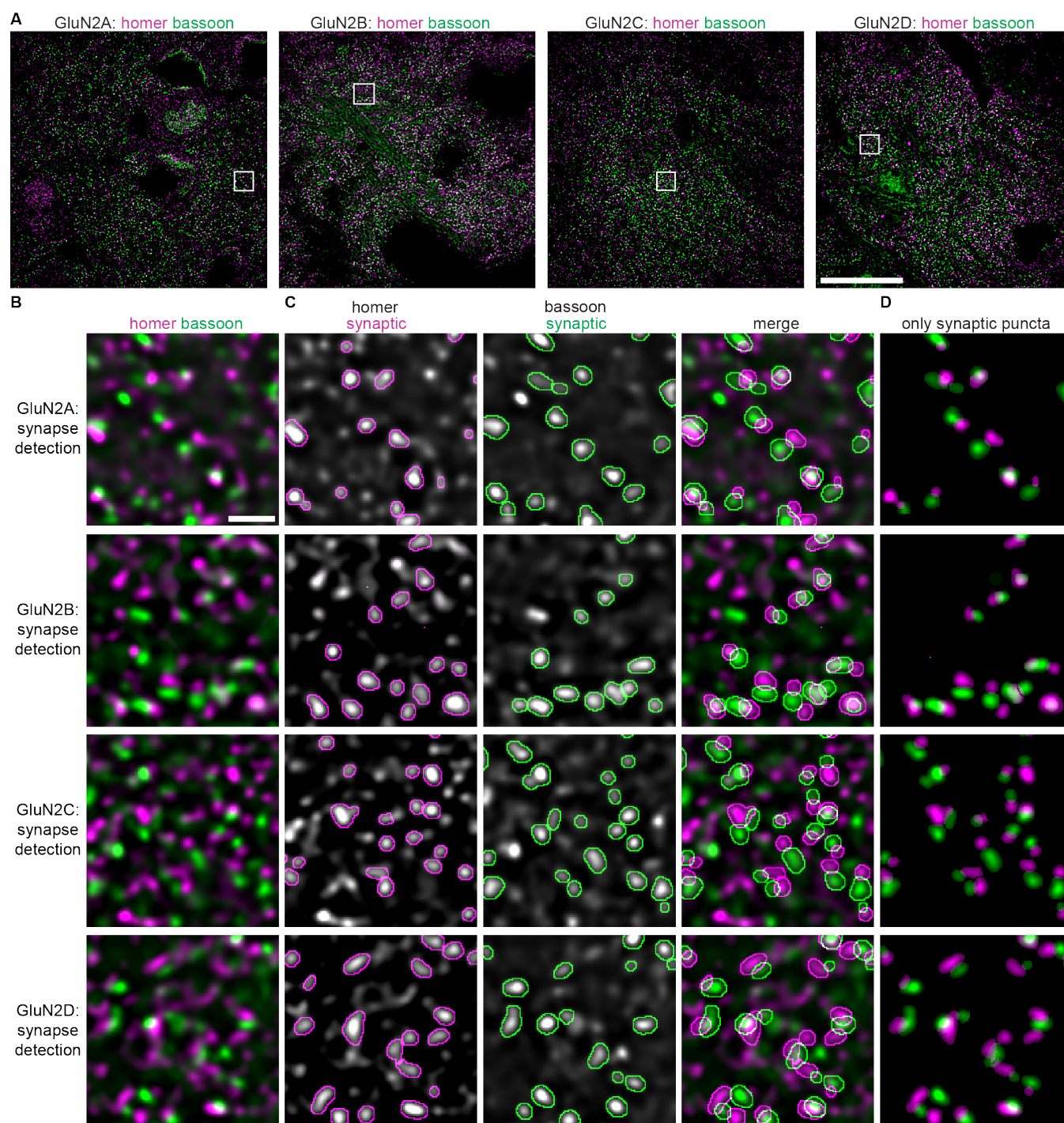
Supplemental Figure S8. Homer-bassoon synapse detection for synaptic GluN2 localization (Figure 3). **A.** 60x images (4x SoRa) show homer and bassoon puncta from respective GluN2A – GluN2D images in Figure 3. **B.** The boxed regions from panel A show individual homer and bassoon puncta. **C.** Homer and bassoon signals from panel B are shown separately in grayscale and merged with outlines depicting all detected postsynaptic homer and presynaptic puncta. The thresholded "only synaptic puncta" image shows only the outlined bassoon and homer puncta. Scale bars: A) 20 µm; B) 1 µm.
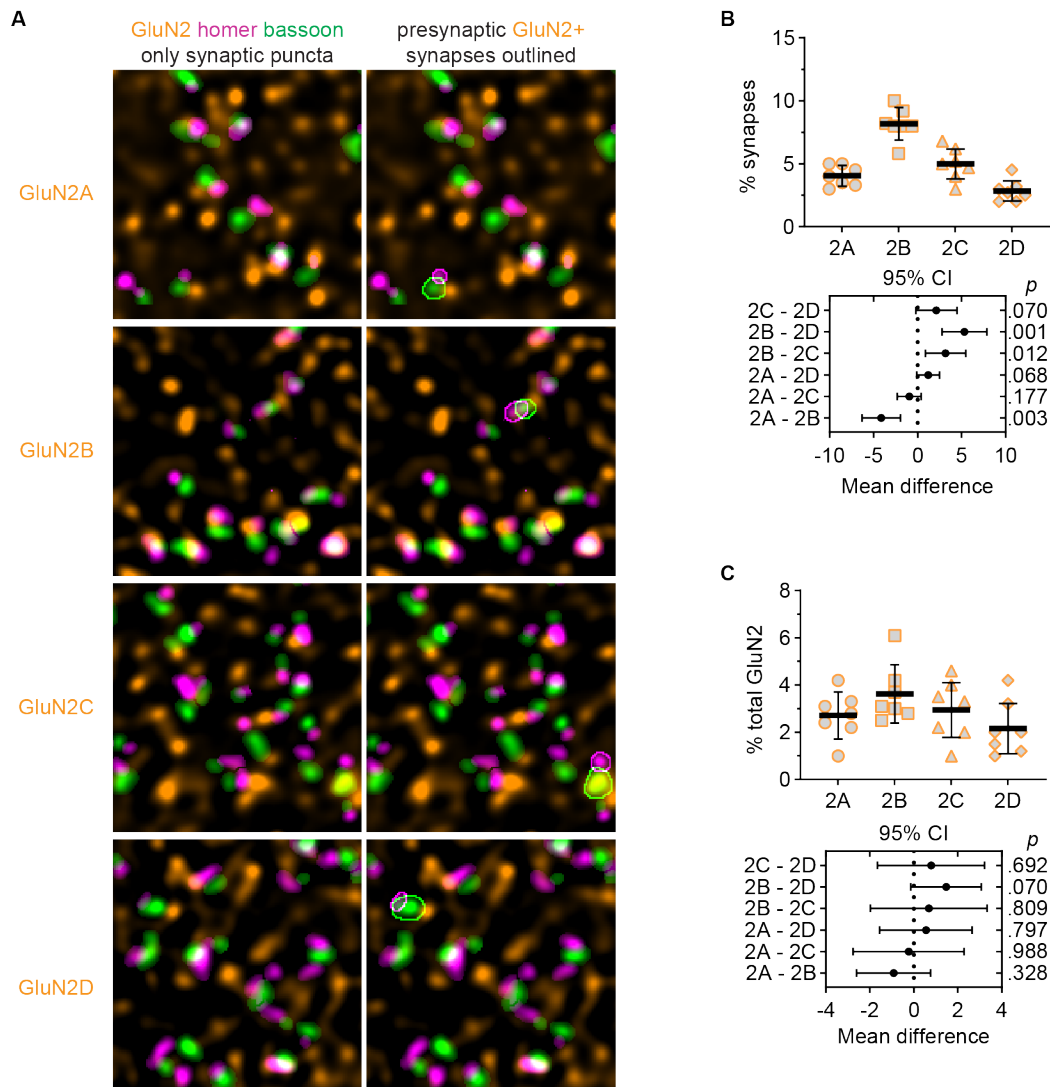
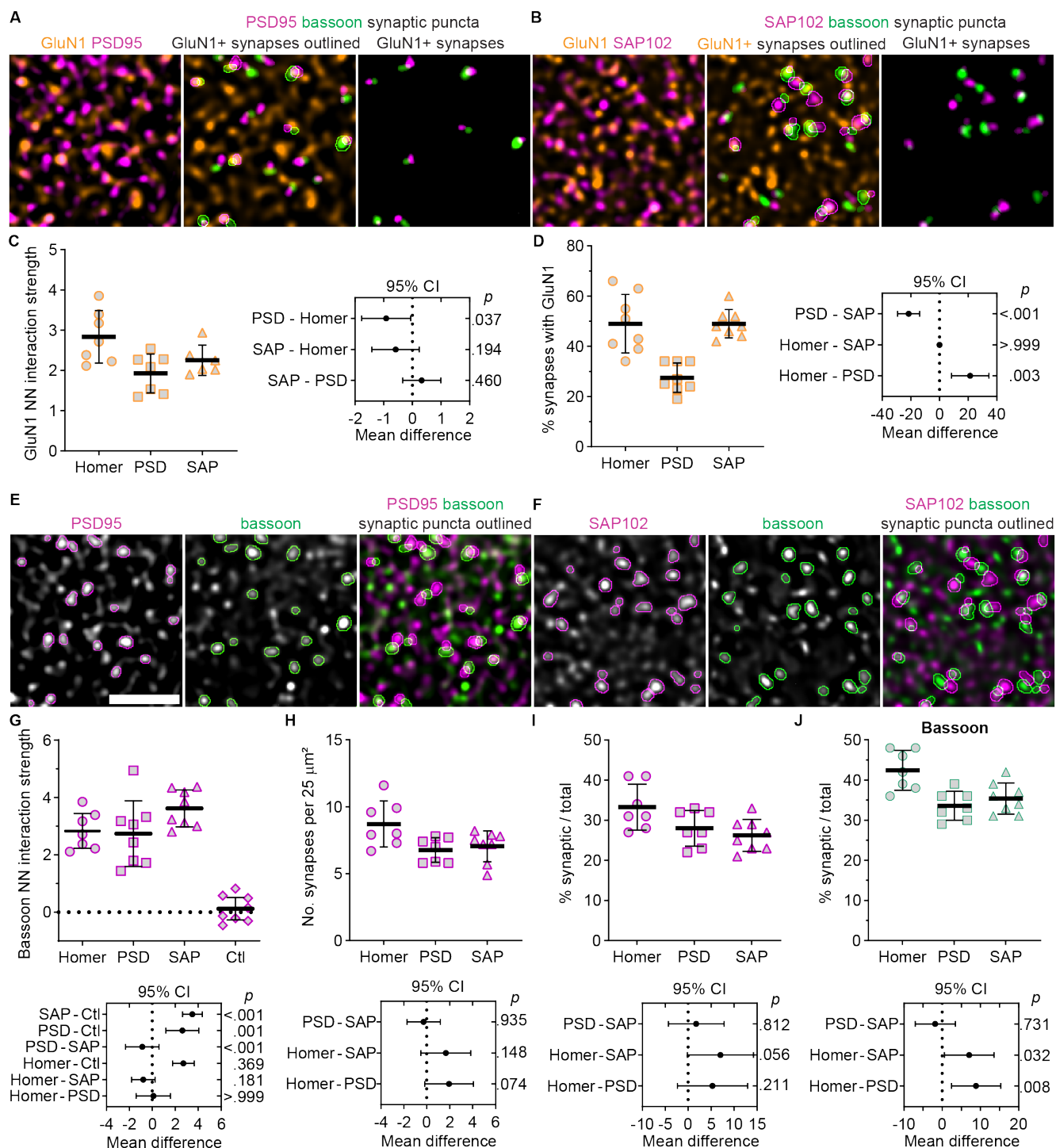**Supplemental Figure S9. Presynaptic GluN2 localization. A.** 60x (4x SoRa) images show GluN2A – GluN2D immunolabeling with synaptic homer and bassoon puncta (same regions as shown in Figure 3). At right, synaptic puncta with GluN2 overlapping presynaptic bassoon without overlapping postsynaptic homer are outlined. **B**. The percentage presynaptic bassoon overlapping GluN2 and **C**) the percentage of GluN2 overlapping presynaptic bassoon were quantified in the full FOV, averaged across three images per mouse, and plotted with group mean ± *SD* (n = 7 mice; 4F, 3M). Data were analyzed with a mixed effects model and Tukey's pairwise comparisons for which the 95% CI fo the mean difference are plotted beneath the group data with the *p* values on the right y-axis. **B:** $F(2.11, 16.9) = 30.9$, $p < 0.001$, n = 7 (4F, 3M); **C**) $F(2.34, 18.7) = 1.91$, $p = 0.171$.
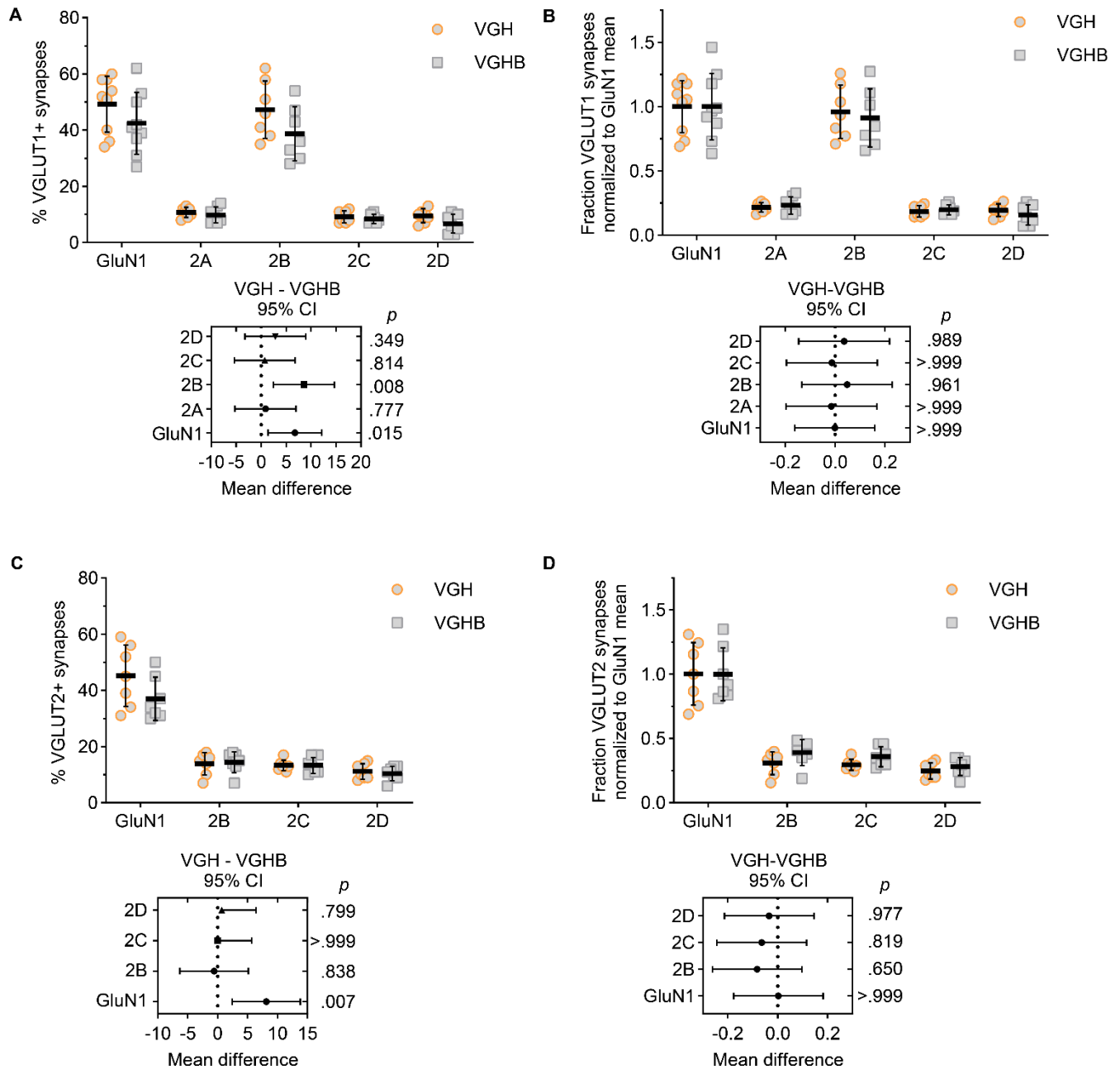
Supplemental Figure S10. Comparison of fraction VGLUT-positive synapses with GluN with and without bassoon. A. The fraction of VGLUT1-positive synapses with GluN2 overlapping homer was measured for immunostainings of VGLUT1, GluN, and homer (VGH) or VGLUT1, GluN, homer, and bassoon (VGHB). VGH defined postsynaptic homer as those homer puncta overlapping VGLUT1, while VGHB defined postsynaptic homer as homer puncta within homer-bassoon pairs with bassoon overlapping VGLUT1. The percentages of synapses with GluN1 and GluN2B significantly differed between these two methods as determined by a mixed-effects model (main effects, GluN: $F_{(1,32)} = 9.07$, p = .005; interaction: $F_{(4, 32)} = 1.46$, p = .237) with posthoc Sidak's tests comparing VGH and VGHB values for each GluN subunit. **B.** The values in panel A were normalized to the GluN1 mean within each group (VGH and VGHB) and the data were analyzed by mixed-effects model to determine if the relative differences between GluN subunits differed between the two methods (main effect, GluN: $F_{(1, 32)} = 0.147$, $p = 0.704$; interaction: $F_{(4, 32)} = 0.192$, $p = 0.941$; n = 7 mice; 4F, 3M). There were no significant differences between the relative values for each GluN subunit. VGLUT2 data shown in panels C and D were analyzed as described for VGLUT1 data. GluN2A was not included because four-channel imaging was not possible with our antibody combinations. **C.** Mixed-effects model, main effect, GluN: $F_{(1, 24)} = 2.24$, $p = .148$; interaction: $F_{(3, 24)} = 2.17$, $p = .117$. **D.** Mixed-effects model, main effect, GluN: $F_{(1, 24)} =$

1.76, $p = .197$; interaction: $F (3, 24) = 0.312$, $p = .817$; n = 7 mice; 4F, 3M. There were no significant differences in the relative values for each GluN subunit.

Supplemental Figure S11. Comparison of synapse detection and GluN1 colocalization with homer, PSD95, and SAP102. 60x (4x SoRa) images show GluN1 with postsynaptic markers (**A**) PSD95 or (**B**) SAP102, GluN1 with synaptic puncta and GluN1-positive synapses outlined, and only GluN1-positive synapses. **C.** The NN interaction strength for GluN1 with homer, PSD95, and SAP102 and (**D**) the percentage of synapses with GluN1 overlapping the postsynaptic marker were plotted with the group ± *SD*. The data were analyzed by mixed-effects models with pairwise Tukey's comparisons for which the 95% CI of the mean difference is plotted (at right) with *p* values on the right y-axis. C: $F (2, 14.95) = 5.593$, p

= 0.015. D: F (2, 13.8) = 18.3, $p < 0.001$. 60x (4x SoRa) images show (**E**) PSD95 and (**F**) SAP102 immunostaining with bassoon in grayscale and the merge with the puncta detected as synapses outlined. The following data were plotted with the group mean $\pm$ *SD*, and analyzed by mixed effects models and Tukey's pairwise comparisons for which the 95% CI of the mean difference is plotted (bottom) with p values on the right y-axis: **G**) NN interaction strength for bassoon with homer, PSD95, and SAP102 as well as bassoon with homer signal rotated 90 degrees (F (3, 18.4) = 31.2, $p < 0.001$), **H**) the number of synapses detected as pairs of bassoon with homer, PSD95, and SAP102 per 25 μm^2 (F (2, 14.1) = 4.56, $p = 0.030$), **I**) the percentage of total homer, PSD95, and SAP102 puncta detected as synaptic (F (2, 16.5) = 4.24, $p = 0.033$), and **J**) the percentage of total bassoon puncta detected as synaptic when paired with homer, PSD95, and SAP102 (F (2, 17.0) = 8.79, $p = 0.002$).

Supplementary Table S1. Hypothesis testing for interaction strength. P values were generated by the Mosaic IA plugin to determine if the interaction strength between bassoon and homer or bassoon with homer rotated 90 degrees (control) were significantly different than randomized coordinates.

Homer/bassoon		Control (homer rotated 90)	
Interaction strength	p value	Interaction strength	p value
2.68	<.001	-0.45	0.676
1.71	<.001	0.83	0.968
2.19	<.001	-0.13	0.133
1.89	<.001	-0.30	0.458
2.53	<.001	0.49	0.849
2.00	<.001	-0.21	0.619
2.53	<.001	0.16	0.334
3.27	<.001	0.58	0.981